MATHEMATICAL BIOSCIENCES
AND ENGINEERING
Volume **8**, Number **2**, April **2011**

doi:10.3934/mbe.2011.8.325

pp. **325–354**

A MODEL OF COMPETING SATURABLE KINETIC PROCESSES WITH APPLICATION TO THE PHARMACOKINETICS OF THE ANTICANCER DRUG PACLITAXEL

Rebeccah E. Marsh

Department of Physics
University of Alberta, Edmonton, Alberta, T6G 2J1, Canada

Jack A. Tuszyński

Department of Physics
University of Alberta, Edmonton, Alberta, T6G 2J1, Canada
and
Division of Experimental Oncology
Cross Cancer Institute, Edmonton, Alberta, Canada

Michael Sawyer

Department of Experimental Oncology
Faculty of Medicine and Dentistry
University of Alberta, Edmonton, Alberta, T6G 2J1, Canada
and
Division of Medical Oncology
Cross Cancer Institute, Edmonton, Alberta, Canada

Kenneth J. E. Vos

Department of Physics and Astronomy
University of Lethbridge, Lethbridge, Alberta, T1K 3M4, Canada

Abstract. A saturable multi-compartment pharmacokinetic model for the anti-cancer drug paclitaxel is proposed based on a meta-analysis of pharmacokinetic data published over the last two decades. We present and classify the results of time series for the drug concentration in the body to uncover the underlying power laws. Two dominant fractional power law exponents were found to characterize the tails of paclitaxel concentration-time curves. Short infusion times led to a power exponent of -1.57 ± 0.14, while long infusion times resulted in tails with roughly twice the exponent. Curves following intermediate infusion times were characterized by two power laws. An initial segment with the larger slope was followed by a long-time tail characterized by the smaller exponent. The area under the curve and the maximum concentration exhibited a power law dependence on dose, both with compatible fractional power exponents. Computer simulations using the proposed model revealed that a two-compartment model with both saturable distribution and elimination can reproduce both the single and crossover power laws. Also, the nonlinear dose-dependence is correlated with the empirical power law tails. The longer the infusion time the better the drug delivery to the tumor compartment is a clinical recommendation we propose.

2000 *Mathematics Subject Classification.* Primary: 92C45, 80A30; Secondary: 34-02.

Key words and phrases. Pharmacokinetic modeling, paclitaxel, nonlinear differential equations, multi-compartment model, Michaelis-Menten kinetics.

This work is supported by NSERC of Canada.

1. Introduction.

1.1. **Pharmacokinetics.** Pharmacokinetics is the study of the absorption, distribution, metabolism, and eventual elimination (ADME) of a drug from the body [17]. Pharmacological data usually consist of discrete values of the concentration of a drug in the plasma as a function of time. For drugs administered by direct intravenous (IV) infusion, a plot of these values generates a concentration versus time curve that rises during the infusion and then decreases after a maximum concentration value is reached. This decline may be relatively short or may last for several days, and it is mainly governed by the rate of elimination of the drug from the body. One of the key questions investigated is the functional dependence of the elimination curve and a single parameter is often used that characterizes the drug, namely its half-life. Our interest is also focused on the power law exponent of the elimination curve since it can provide important information about the fate of the drug in the body and its efficacy. During clinical trials, the concentration-time curves are used to determine optimum dosing regimens, potential toxicities, and drug-drug interactions. One of the major challenges in dose optimization is nonlinear behavior in one or more drug processes. In this study, we investigate new ways to assess and quantify nonlinear pharmacokinetic behavior using empirical power laws, with emphasis on their origins and diagnostic applications to the drug paclitaxel.

1.2. **Paclitaxel.** Paclitaxel, derived from the bark of either the Pacific Yew tree or the European Yew tree [51], is one of the most important anticancer drugs developed in the past two decades. It is active against many human solid tumours related to breast cancer, ovarian cancer, non-small lung cancer, head and neck cancer and advanced forms of Kaposi's sarcoma [20]. Paclitaxel is also used for the prevention of restenosis. Because it is poorly water-soluble, the current formulation Taxol® incorporates a 6 mg/ml solution in a solvent consisting of 50%® polyoxyethylated castor oil (Cremophor® EL-CrEL) and 50% dehydrated alcohol (USP). Paclitaxel is typically administered by intravenous infusion over one or three hours but has also been administered over six and twenty four hours. Because a patient may have an anaphylactic reaction to CrEL, alternative formulations of paclitaxel have been introduced, including BMS-184476, oral paclitaxel in polysorbate 80, and ABI-007, Genexol-PM [27] and Abraxane® (nab-paclitaxel) [49]. Paclitaxel has a long residence time within the body and can stay trapped in cancer cells for over a week [37]. Paclitaxel is also highly bound to CrEL micelles, plasma proteins, platelets, and red blood cells [19].

1.3. **Molecular action of taxol.** Paclitaxel is a mitotic inhibitor, which binds preferentially to microtubules, which are cellular components necessary for mitosis, intracellular transport, maintenance of cell shape, and cellular motility. Usually, there is a dynamic balance between microtubules and their building blocks, tubulin, free in solution. By shifting the balance towards microtubule polymerization, however, cell replication is strongly inhibited during the G2 and M phases of the cell cycle [45, 22]. *In vitro*, paclitaxel binds reversibly to microtubules with an affinity of approximately 1 μM and a stoichiometry of one paclitaxel molecule per α/β tubulin dimer. In the body, paclitaxel is highly bound to plasma proteins (95 - 98%), and it is eliminated through metabolism in the liver by cytochrome P-450 enzymes CYP3A4 and CYP2C8 [36]. Paclitaxel's mechanism of action results in the inhibition of cell replication causing cell death due to apoptosis [23]. A family of related

compounds known as taxanes, including the drug docetaxel, has been developed to improve upon the successful therapeutic properties of paclitaxel for example by increasing its specificity and water solubility; in addition the epothilones, another family of anti-cancer drugs, are believed to bind at the taxol active site [40, 47].

The binding site of taxol is located on the β-tubulin unit within the α/β heterodimer, the repeating element forming the long protofilaments that together make up the hollow, cylindrical microtubule structure. Figure 1 shows paclitaxel (panel a) and docetaxel (panel b) bound to β-tubulin while panel c illustrates its binding site location on a microtubule protofilament relative to the other two anti-mitotic drugs: vinblastine and colchcicine. The shortening and lengthening of microtubules, called the dynamic instability, is necessary for the formation of the mitotic spindle during cell division, of which microtubules are the main components. Shortening occurs when the GTP nucleotides linking individual dimers become hydrolyzed to GDP, causing dimers to depolymerize from the ends of microtubules. Binding of paclitaxel to tubulin locks these building blocks in place and the resulting microtubule/paclitaxel complex does not have the ability to disassemble. When taxol binds to microtubules at a site in the microtubular lumen or interior, it modifies the dynamic properties of the microtubule, leading to stabilization of GDP-bound tubulin against depolymerization [24]. This adversely affects cell function because the dynamic instability of microtubules is necessary for the cell's proper functioning as a mechanism to transport other cellular components. For example, during mitosis, microtubules position the chromosomes during their replication and subsequently lead to the separation into two daughter-cell nuclei [53]. This destroys the cell's ability to use its cytoskeleton in a flexible manner. Further research has indicated that paclitaxel induces programmed cell death (apoptosis) in cancer cells by binding to an apoptosis inhibiting protein called Bcl-2 (B-cell leukemia 2) and thus arresting its function. In addition to stabilizing microtubules paclitaxel may act as a molecular mop by sequestering free tubulin effectively depleting the cell's supply of tubulin dimers. This activity may trigger the aforementioned apoptosis [25].

One common characteristic of most cancer cells is their rapid rate of cell division. In order to accommodate this, the cytoskeleton of a cell undergoes extensive restructuring. Paclitaxel is an effective treatment for aggressive cancers because it adversely affects the process of cell division by preventing this restructuring. Cancer cells are also destroyed by the aforementioned anti-Bcl-2 mechanism. Some normal cells are also affected adversely, for example immune system cells, neurons and epithelial cells, but since cancer cells divide much faster than non-cancerous cells, they are far more susceptible to paclitaxel treatment resulting in an overall therapeutic benefit to the patient.

1.4. **Objectives and organization of the paper.** The main objective of this paper is pharmacokinetic model development intended to capture various sources of data on the pharmacokinetics of paclitaxel, especially the dependence of the concentration of the drug in blood plasma on the infusion time, which has been shown to exhibit bi-phasic behavior. We will analyze the concentration versus time data from as many published experimental studies as possible to create a general mathematical model of paclitaxel pharmacokinetics broadly based on the available information. Once the model has been built, we intend to investigate its solutions both numerically and analytically. We have developed a three-compartment saturable model that can be simplified to a two-compartment saturable model without

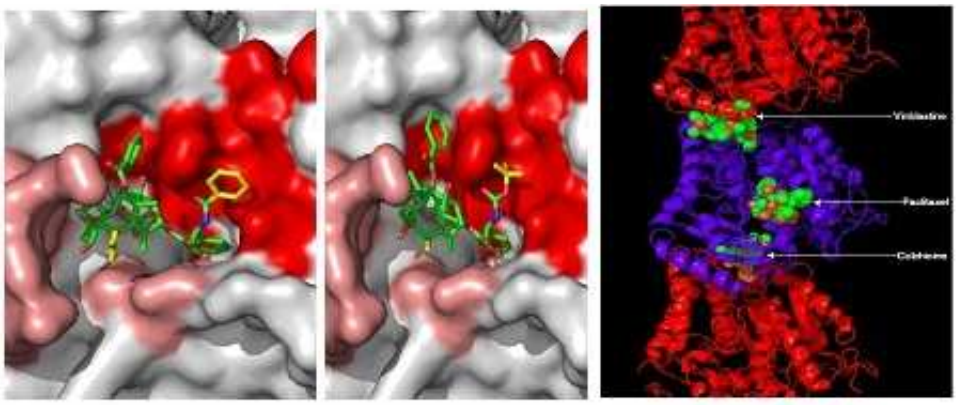

FIGURE 1. Illustration of the molecular binding of paclitaxel (panel a) and docetaxel (panel b) bound to β tubulin while panel c illustrates its binding site location on a microtubule protofilament relative to the other two anti-mitotic drugs: vinblastine and colchcicine.

loss of generality under prevailing kinetic conditions. We have applied both analytical and numerical approaches aimed at analyzing and explaining the origin of power laws shown by the concentration versus time curves. While the qualitative aspects of the model and its preliminary analysis were published elsewhere [34], the current paper presents a detailed description of the mathematical development of the model and its solutions within the context of its pharmacokinetic relevance. It is recognized that in the context of biological phenomena, the inference of power laws should involve several decades on the time axis. While in our case, or in pharmacokinetics in general, such long-term observations are simply impossible due to short half-life times of drug entities in the human body, paclitaxel has an unusually long time scale of elimination spanning at least two or even three orders of magnitude (from minutes to days). Therefore, with clearly distinct functional profiles from classical exponential decay in pharmacokinetics, we strongly believe the use of power laws is justified in this case.

In the next section we systematically analyze experimental data extracted from various sources according to the control parameters (infusion time, dose) and group them accordingly to find characteristic properties of the data sets and the underlying mechanisms of paclitaxel activity in the body. We look for the key properties of paclitaxel pharmacokinetics by studying the area under the curve (AUC), half-life and the maximum concentration (C_{max}). We define the concentration of the drug in the blood as both a function of time t and total dose D, C(t,D). We can then define two pharmacokinetic quantities relevant to high-dose chemotherapeutic drugs: the AUC (holding the dose D constant):

$$AUC = \int_0^\infty C(t)dt \tag{1}$$

and C_{max}, the maximum concentration reached in the blood:

$$C_{max} = C(t, D)|_{\frac{dC}{dt}=0} \tag{2}$$

Datasets from various studies were taken from the literature. Graphs of pharmacokinetic profiles were digitized, while AUC and C_{max} values were taken directly from tables.

In Section 3, we develop a pharmacokinetic model using initially a saturable three-compartment model where the compartments represent: (a) the blood plasma including the organs of elimination, e.g. the liver, (b) the tumor compartment and (c) an optional compartment that involves drug binding with other organs that are neither eliminating the drug nor part of the tumor. These could be plasma proteins or organs rich in tubulin such as the brain or epithelial structures. We then argue that combining the elimination compartment with the blood plasma compartment is a reasonable simplification in view of the values of the kinetic coefficients involved. This section is further subdivided into three subsections that deal with: 3.1 model development, 3.2 numerical analysis of the data, and 3.3 analytical investigations including some exact solutions. The last section of the paper summarizes our findings with practical suggestions for optimal drug dosage and infusion times due to the insights gained in this work into paclitaxel distribution, binding and elimination.

2. Analysis of the experimental data.

One of the main challenges with administering paclitaxel is its observed dose-dependence; a given increase in dose results in a greater than proportional increase in both C_{max} and AUC of the drug. In addition, compartment models with linear rate constants provide less than adequate fits to the pharmacokinetic profiles. As a result, two-compartment and three-compartment models were introduced with saturable Michaelis-Menten kinetics incorporated into both the distribution and elimination [53, 26, 16]. The same studies all observed that the C_{max} and AUC values for paclitaxel in patients increase disproportionately with an increase in dose, although the relationships were less evident for the longer, twenty four-hour infusions. Furthermore, the rate constant for elimination was much higher than that for distribution (Kearns *et al.*[26] found a seventeen-time greater value).

There is evidence that concentration versus time curves for many drugs, including paclitaxel, exhibit long-time power law tails of the form

$$C(t) \sim t^{\alpha};\ t > T, \tag{3}$$

where T marks the onset time and α is the negative power exponent. However, these curves are not adequately modeled by single processes such as straight-forward linear absorption or elimination. In this article, we demonstrate how a multi-compartment model with two Michaelis-Menten processes [35] of saturable binding and elimination can produce both single and dual power law tails with characteristic negative exponents.

It is worth mentioning that negative power laws were first applied empirically to describe the washout of bone-seeking radioisotopes [41, 66]. Subsequently, other types of clearance curves have been fitted by a single power law, two sequential power laws, or the gamma function, $y(t) = a_1 t^{-a_2} e^{-a_3 t}$. [2, 3, 42, 65] Although most of these applications of the power law have been strictly empirical, several explanatory models have been proposed including: a stochastic random walk model based on molecules cycling in and out of the plasma [64], a set of convection-diffusion equations for transit in the liver [42], gamma-distributed drug residence times [61], and fractal elimination kinetics under both homogeneous and heterogeneous conditions [7, 33, 9, 10, 58, 59]. In addition, Beard and Bassingthwaighte [4] showed that

a sum of scaled exponential functions can produce power law behavior. However, a model based on this assumption would necessarily imply a well-stirred compartment situation without saturation. Therefore, while exponential functions could be used for retrospective fits to data points, in our opinion this type of modeling would have limited applicability for long-term trend representation and, especially for prospective modeling not to mention their limited explanatory power. We believe that in the case of paclitaxel pharmacokinetics conditions of saturable concentrations as well as non-homogeneous compartments apply, hence the importance of power-laws is clear. In parallel, power law relationships between pharmacokinetic variables have also emerged in fractal models that describe enzyme kinetics occurring within heterogeneous environments [29, 28, 31].

Power laws have also been used to model dose-proportionality of pharmacokinetic parameters, such as the AUC and the C_{max}. If a doubling of the dose of a drug produces no change in the values of the pharmacokinetic parameters, the system is dose-independent. If a doubling of the dose produces a doubling of one or more pharmacokinetic parameters, the system is considered to be dose-proportional (linear). If the parameter decreases or increases by a factor other than two, the system is considered to be nonlinear. To quantify the extent of nonlinear dose-dependence, Gough *et al.* [18] proposed the "power model":

$$P \sim cD^{\beta}, \tag{4}$$

where P represents the pharmacokinetic parameter and D is the dose. However, the authors only considered cases corresponding to $\beta = 0$ (dose-independence) and $\beta = 1$ (linear dose-dependence). Their solution for fitting a nonlinear relationship was the addition of higher-order polynomial terms to equation 4. In addition, the authors stressed that their model is empirical and that their application of the power law was not mechanistic. To the best of our knowledge, a critical consideration of noninteger values of β has yet to be made. Here, we report such values and attempt to relate them to characteristics of the concentration versus time curve.

To this end, forty-one sets of concentration versus time data from twenty published clinical trial studies were included and digitized using Macromedia Fireworks Version 4 (San Jose, California). The data were tested for power law tails of the form expressed by equation 3, where T coincides with the end of the IV infusion of paclitaxel. Regression analysis was performed on log-log data, with the goodness of fit evaluated using the coefficient of determination, R^2. The mean number of data points in the tail was 9 ± 2 (minimum of 6 and maximum of 13). Eight sets of AUC and C_{max} data were taken directly from ten published studies and were fit to equation 4. The mean number of dose levels per study was 4 ± 1 (minimum of 3 and maximum of 6). Thirty-nine of the forty-one concentration versus time curves exhibited power law tails. Values calculated for the power exponent α are summarized in table 1. Although the exponent was relatively independent of patient characteristics (such as weight, age, sex, and the type and stage of cancer) and the dose level, it varied with the length of the infusion. For short infusions (one hour duration), a single long-time tail was observed with a power exponent of $\alpha = -1.57 \pm 0.14$. The tails persisted up to twenty-four hours and in one case up to thirty-six hours. For long infusions (six hours or twenty-four hours duration), a single long-time tail was also observed but with an exponent of over 3. The tails extended up to twenty-four hours for the six-hour infusions and up to forty-eight hours for the twenty-four-hour infusions.

TABLE 1. The power law exponent α quantifying the tails of paclitaxel concentration curves. [1, 32, 38, 14, 43, 26, 16, 56, 52, 13, 39, 55, 57, 15, 11, 19, 6, 62, 67, 63, 53, 44]

Infusion Time (h)	Dose Range (mg/m^2)	Initial α	Slope R^2	Terminal α	Slope R^2
1	150			-1.25 – -1.59	
1	175			-1.40 – -1.68	
1	200			-1.58 – -1.61	
1	225			-1.50 – -1.67	
1	250			-1.69 – -1.71	
AVG	150 – 250			-1.57 (0.14)	0.97 (0.02)
3	60	-6.56 (0.41)	0.989	-1.22 (0.13)	0.959
3	105	-3.57 (0.71)	0.863	-1.63 (0.14)	0.944
3	135	-3.04 – -3.38		-1.56 – -1.72	
3	150	-3.08 (0.47)	0.956	-1.87 (0.04)	0.998
3	175	-2.85 – -3.94		-1.14 – -1.84	
3	180	-3.14 (0.50)	0.908	-1.61 (0.04)	0.996
3	225	-3.19 – -3.67		-1.77 – -1.79	
3	240	-3.37 (0.42)	0.942	-1.70 (0.06)	0.991
3	250	-3.30 – -3.34		-1.74 – -1.78	
3	290			-2.29 – -2.72	
AVG	150 – 250	-3.38 (0.27)	0.95 (0.04)	-1.70 (0.16)	0.99 (0.02)
6	175			-3.35 (0.25)	0.962
6	230			-1.22 (0.08)	0.987
6	250			-3.40 (0.23)	0.955
6	275			-2.46 (0.13)	0.968
AVG	175 – 275			-3.07 (0.53)	0.96 (0.01)
24	105			-1.97 (0.09)	0.991
24	180			-2.62 (0.09)	0.996
24	250			-3.06 (0.18)	0.981
24	275			-3.69 (0.69)	0.851
24	290			-3.37 (0.27)	0.977
24	350			-3.35 (0.21)	0.988
24	825			-3.41 (0.18)	0.981
AVG	180 – 290			-3.23 (0.55)	0.94 (0.08)

In contrast, for the intermediate infusion time of three hours, the concentration versus time curves exhibited a crossover between two power law regimes. At the end of the infusion phase, there was an initial period of one to two hours where the slope has a power exponent, which is equal within error to the slope exhibited by the six-hour and twenty-four-hour infusion curves. This initial slope was followed by a long-time tail with a power exponent equal within error to that exhibited by the one-hour infusion curves. The length of the long-time tail ranged from nine to sixty-eight hours post-infusion. Figure 2 shows the distinct dual nature of the tails for three-hour infusions of paclitaxel. In addition, the rise of each curve also appears to follow a power law relationship. In pharmacokinetics, the shape of the curves is called a flip-flop situation because the initial slope is steeper than the terminal

long-time tail. One would expect the opposite, since smaller plasma concentrations should be cleared more rapidly. Usually, a flip-flop is linked to orally-administered drugs whose absorption rate constant is smaller than the elimination rate constant [5]. In the case of paclitaxel, however, we believe that the flip-flop is associated with the distribution of drug from the plasma to other tissues especially the tumor compartment.

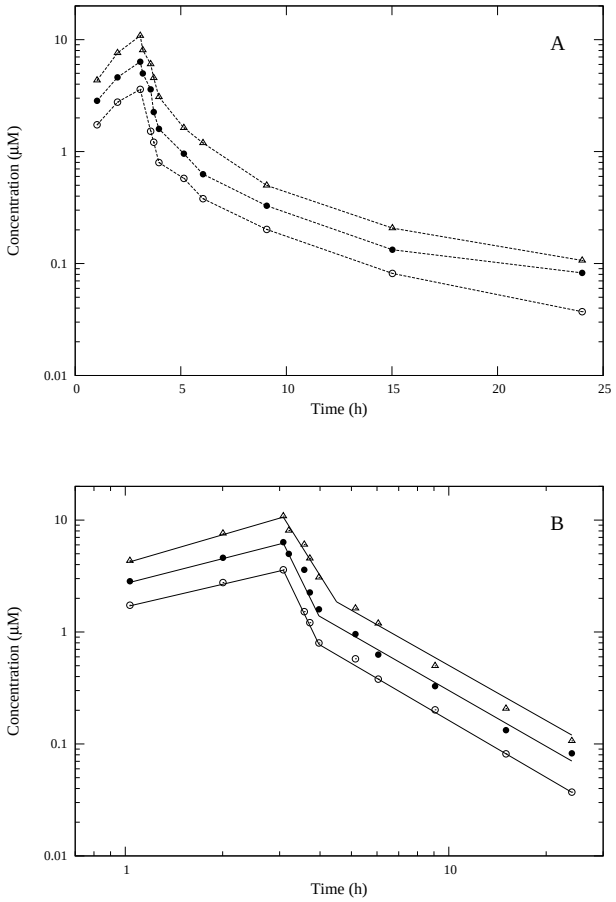

FIGURE 2. Pharmacokinetic data obtained for three-hour infusions of paclitaxel, replotted from Kearns *et al.* [26] for three dose levels (open circles, $135mg/m^2$; solid circles, $175mg/m^2$; open triangles, $225mg/m^2$). (A) Log-Lin plot showing the non-exponential nature of the tails of the curves. (B) Log-log plot showing three distinct power law regions.

The observed power law behavior is likely not a consequence of binding to the CrEL formulation vehicle or blood components but of the saturable processes at play as discussed above. This is evidenced by the fact that analysis of two CrEL-free formulations of paclitaxel produced results consistent with those observed for regular paclitaxel. Two concentration versus time curves for thirty-minute infusions

TABLE 2. The slope of $ln(AUC)$ versus $ln(dose)$ illustrating the paclitaxel dose-dependence. [1, 32, 15, 56, 7, 33, 11]

Infusion Time (h)	Dose Range (mg/m^2)	Slope	R^2
1	150 – 250	1.84 (0.17)	0.975
1	150 – 250	1.85 (0.32)	
3	54 – 94.5	1.61 (0.46)	0.862
3	105 – 270	1.65 (0.12)	0.978
3	135 – 175	1.57 (0.28)	0.970
3	135 – 300	1.84 (0.16)	0.997
6	175 – 275	1.65 (0.63)	0.774
24	54 – 94.5	1.61 (0.46)	0.862

of the drug ABI-007 taken from Damascelli *et al.* [8] demonstrated single power law tails with $\alpha = -1.61$. Four curves for three-hour infusions of $175 - 390\ mg/m^2$ of the drug Genexol-PM taken from Kim *et al.*[27] exhibited dual power law tails with $\alpha = -4.99 \pm 0.57$ for the initial slope and $\alpha = -1.65 \pm 0.15$ for the terminal slope. The concentration versus time curve reported by van Zuylen *et al.*[57] for paclitaxel in whole blood following a three-hour infusion produced an initial power exponent of $\alpha = -3.86 \pm 0.59$ and a terminal exponent of $\alpha = -1.64 \pm 0.01$.

We conjecture that the steep curves (described by the larger power exponent) correspond to the case where the distribution process is not saturated, allowing the maximum fraction of drug to be distributed outside the blood plasma. This situation occurs when the drug is infused relatively slowly. The shallow curves, however, result when the distribution process is saturated, and therefore the smaller power exponent predominantly reflects the elimination process. This situation occurs when the drug is infused relatively rapidly. The fact that the power law tails persist even at low concentrations (below the reported K_M values) provides additional information about the system. This continued adherence to a power law indicates a failure of the drug to attain a steady state in the peripheral compartment(s). Therefore, drug distribution to and release from the tissues plays a dominant role in the pharmacokinetics of paclitaxel at all plasma concentrations.

We should qualify the above statements with the following comment. Due to the natural limitations to the quantification of the drug concentration, the empirical power laws described here are only valid over one to two decades. Therefore, the term power law as used in this article technically refers to an empirical characteristic. Nonetheless, the empirical power exponents have practical and clinical significance because they allow us to distinguish between different regimes of a process.

The dose-dependence of AUC and C_{max} were found to be nonlinear, in agreement with the literature, as shown in tables 2 and 3. The relationship in equation 4 provided a good fit to the data, and the results are listed in table 4. The two values of β agree within error with each other and with the exponent characterizing the shallow long-time tails. Note that these results are only valid over the therapeutic dose ranges considered, and caution should be used in extrapolating beyond this range.

After confirming the existence of power law tails in paclitaxel concentration versus time curves, we wanted to test whether they could be generated using a model

TABLE 3. The slope of $ln(C_{max})$ versus $ln(dose)$ illustrating the paclitaxel dose-dependence. [1, 32, 56, 7, 33, 11, 63, 67]

Infusion Time (h)	Dose Range (mg/m^2)	Slope	R^2
1	150 – 250	1.87 (0.35)	0.904
1	150 – 250	1.86 (0.19)	0.918
3	105 – 270	1.66 (0.15)	0.969
3	135 – 175	1.64 (0.36)	0.955
3	135 – 300	1.66 (0.12)	0.984
6	175 – 275	1.74 (0.78)	0.713
24	200 – 275	1.70 (0.31)	0.968
24	250 – 390	1.82 (0.54)	0.919

TABLE 4. The power law exponent β quantifying the dose dependence of pharmacokinetic parameters for one-hour paclitaxel infusions. The number of data sets is eight. [26, 16, 32, 38, 43, 56, 62, 50, 63, 46]

Parameter	Dose Range (mg/m^2)	β	R^2
AUC	54 – 300	1.76 (0.17)	0.94 (0.08)
C_{max}	135 – 390	1.74 (0.09)	0.92 (0.09)

involving the competition between two saturable processes arising in the tumor compartment and the elimination (combined liver and blood plasma) compartment. Below we provide a mathematical description of the model proposed here. The main building blocks of the model and some numerical analysis aimed at reproducing experimental data was first presented by Marsh *et al.* [34]. However, our focus in the present paper is to go beyond the replication of experimental data and hence we intend to provide the reader with an in-depth analytical investigation of the underlying mathematical equations and their solutions.

3. **Theoretical analysis.**

3.1. **Model development.** The most common type of pharmacokinetic model is the compartmental model [21], in which a compartment is defined as the number of drug molecules having the same probability of undergoing a set of chemical kinetic processes. The exchange of drug molecules between compartments is described by kinetic rate coefficients. The number of molecules in a compartment can be converted to a concentration using the concept of the volume of distribution, the theoretical volume into which the drug is dispersed.

Consider a one-compartment model post-infusion, such that

$$\frac{dC}{dt} = -kC, \tag{5}$$

where k is the kinetic rate coefficient describing the elimination process. If the compartment is homogeneous and instantaneously-mixed (well-stirred), the kinetics are classical and

$$k = k_0, \tag{6}$$

where k_0 is a constant. The resulting concentration versus time curve has an exponential tail. Inhomogeneous compartments are typically modeled using fractal kinetics [12] with a time-dependent kinetic rate coefficient:

$$k = k_0 t^{-\eta}, \tag{7}$$

where η is a fractal exponent which could be related to the fractal dimension of the organ in which the process takes place. The resulting concentration versus time curve has a stretched exponential tail. Saturable kinetics are usually modeled using Michaelis-Menten kinetics [35], where

$$\frac{dC}{dt} = -\frac{v_{max} C}{K_M + C}. \tag{8}$$

The quantity v_{max} is the maximum rate of the reaction, and K_M is the concentration required to achieve half the maximum rate of the process. The corresponding concentration versus time curve exhibits an initial linear segment followed by an exponential tail at low concentrations.

Clearly, a single compartment model is insufficient to capture the complexity of the pharmacokinetic data exhibited by paclitaxel. We believe that the simplest non-trivial model required for this purpose is a two-compartment model in which both compartments are saturable due to the limitations on: (a) the number of liver enzymes in the elimination compartment and (b) the molecular targets (i.e. microtubules available for binding) in the tumor compartment. This general scheme is illustrated graphically in figure 3 and described mathematically in equations 9 to 11. Both figure 3 and these equations explicitly contain a third compartment that can be understood as non-eliminating organs that also bind the drug since microtubules are organelles widely distributed in various healthy tissues, especially in the brain. This is, in our opinion, an optional generalization of the model that does not appear to greatly impact the analysis, especially if the kinetic coefficients k_{13} and k_{31} are smaller than k_{12} and k_{21} as one would expect from highly efficacious drugs, such as paclitaxel and docetaxel, that preferentially target the tumor tissue. Therefore, we have decided to proceed with an effective two-compartment model that can be understood to implicitly contain the third compartment through rescaled kinetic coefficients.

Clinical trials indicate that the area under the plasma curve and the maximum plasma concentration for paclitaxel increase disproportionately with an increase in dose. Not surprisingly, compartmental models with linear rate constants have provided less than adequate fits to paclitaxel concentration versus time curves. As a result, two-compartment and three-compartment models with both saturable distribution and saturable elimination have been used to model clinical data [53, 26, 16]. Figure 3 shows the central plasma compartment, transfer to a second compartment via Michaelis-Menten kinetics, and optional transfer to a third compartment via linear kinetics. Saturable distribution has been attributed to either transport [53] or binding [25] processes. The model is described by the following system of equations:

$$\dot{C}_1 = -\frac{v^d_{max} C_1}{K^d_M + C_1} + k_{21} C_2 - k_{13} C_1 + k_{31} C_3 - \frac{v^e_{max} C_1}{K^e_M + C_1} + \frac{i(t)}{V_d}, \tag{9}$$

$$\dot{C}_2 = \frac{v^d_{max} C_1}{K^d_M + C_1} - k_{21} C_2, \tag{10}$$

$$\dot{C}_3 = k_{13} C_1 - k_{31} C_3. \tag{11}$$

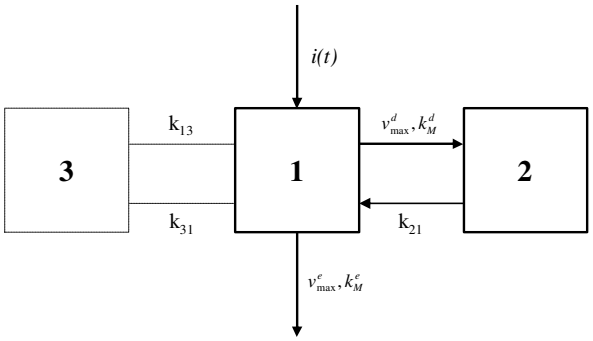

FIGURE 3. The diagrammatic representation of a two-compartment model with both saturable distribution and saturable elimination from the central compartment; as well as an optional third compartment with linear binding.

TABLE 5. Mean population values reported by Kearns *et al.*[26] and the hypothetical values with $K^d_M << K^e_M$ by Marsh *et al.*[34].

Parameter	Kearns' Values	Marsh's Values
v^d_{max}	$10.20\mu M h^{-1}$	$10.0 mg L^{-1}$
K^d_M	$0.32\mu M$	$0.1 mg L^{-1}$
k_{21}	$0.68 h^{-1}$	$0.5 h^{-1}$
v^e_{max}	$18.80\mu M h^{-1}$	$1.0 mg L^{-1}$
K^e_M	$5.50\mu M$	$5.0 mg L^{-1}$
k_{13}	$2.20 h^{-1}$	$0 h^{-1}$
k_{31}	$0.65 h^{-1}$	$0 h^{-1}$
V_d	$4.00 L$	$4.00 L$

The superscript d indicates parameters that describe the distribution process, the e superscript indicates the elimination process, $i(t)$ is the input function (infusion rate), and V_d is the volume of distribution.

Some analytical solutions were obtained for the two-compartment model illustrated in figure 3, which is discussed in Sec. 3.3 below. As well, computer simulations of the two-compartment and three-compartment model illustrated in figure 3 were performed using a fourth-order Runge-Kutta algorithm [48] to numerically solve equations 9 to 11. The parameter values used were those reported by Kearns *et al.*[26] and are summarized in table 5. The molecular weight of paclitaxel is 853.93 g/mol, so the conversion factor between units is $1 mg/L = 1.171\mu M$. The values were not simulated below the quantification limit of paclitaxel (0.005 mg/L [54]). AUC was calculated using Simpson's method, and C_{max} was simply the largest value of C attained during the Runge-Kutta algorithm.

3.2. **Numerical simulations.** We subsequently confirmed that the data shown in figure 2 were best fitted by the model illustrated in figure 3. We indeed found that the Akai Information Criterion (AIC) [30] was lower for both the two-compartment

version ($AIC = -16.3 \pm 3.6$) and the three-compartment version ($AIC = -15.4 \pm 2.9$) than for either a linear two-compartment model ($AIC = -5.8 \pm 1.8$) or a two-compartment model with fractal Michaelis-Menten elimination kinetics [33] ($AIC = -6.5 \pm 2.1$).

Simulations of the model shown in figure 3 with the parameters listed in column 1 of table 5 did indeed replicate the behavior. Figure 4 shows the shape of the concentration versus time curve as a function of the infusion time. For the three-hour infusion, a dual power law tail is evident. As the infusion time decreases, the initial slope becomes longer and less steep, and it is feasible that a single power law may be observable after short infusion times under certain conditions. Conversely, as the infusion time increases, the initial slope becomes shorter until there is a transition to a single steep power law, which occurs for the twenty-four-hour infusion curve. It should be noted that the long-term asymptotic of this model leads naturally to exponential behavior. However, due to the quantification limit of the drug concentration, the transition to an exponential may not be observed.

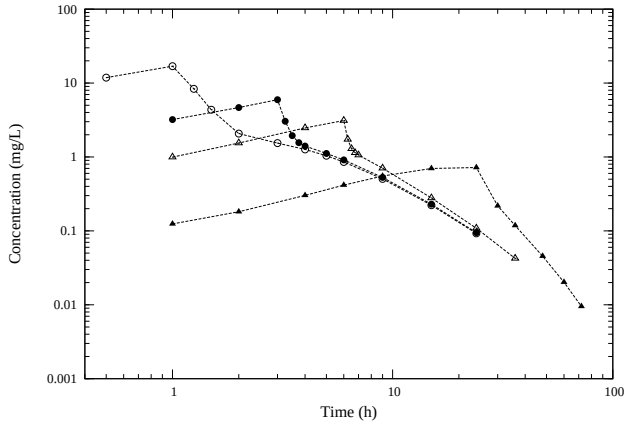

FIGURE 4. The effect of the infusion time on the shape of the concentration versus time curve. Open circles, one hour; solid circles, three hours; open triangles, six hours; solid triangles, twenty-four hours.

An advantage of simulations is that they allow us to perform "virtual experiments" and study the effects of different parameters on the shape of the concentration versus time curve. By perturbing the parameter values, we found that the duration of the initial steep slope is determined by parameters describing the saturable distribution process, v^d_{max} and K^d_M, while the value of the exponent of the initial slope is determined predominantly by the parameters describing the saturable elimination process, v^e_{max} and K^e_M. The slope of the shallow terminal curve is determined mainly by v^d_{max}, where an increase in its value produces an increase in α. This confirms the hypothesis proposed above that the steep curve reflects both the distribution and elimination processes while the shallow curve is dominated by the maximum rate of elimination.

In order to confirm our initial decision to ignore the third compartment we analyzed the effect of its inclusion in the model as a linear binding compartment and found not to have an important effect. For low values of k_{13} (weak binding), the

slopes of the two segments remain unchanged, but the duration of the initial slope increases (Figure 5). As k_{13} becomes larger, however, the long-time tail eventually goes through a transition to an exponential shape. Therefore, an increase in the strength of the linear binding process decreases the plasma concentration and minimizes the effect of the saturable processes.

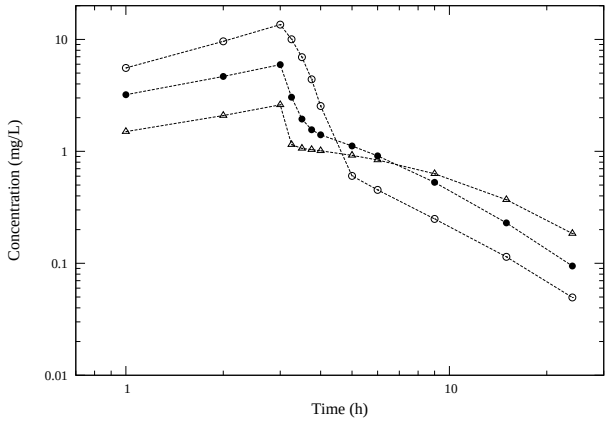

FIGURE 5. The effect of the strength of the linear binding compartment on the shape of the concentration versus time curve. The tail becomes exponential for high k_{13} values. Open circles, $k_{13} = 0h^{-1}$; solid circles, $k_{13} = 2.2h^{-1}$; open triangles, $k_{13} = 8.8h^{-1}$.

In the case of paclitaxel, $K_M^d << K_M^e$, and therefore the distribution process saturates before the elimination process. But what occurs when the reverse, $K_M^d >> K_M^e$, is the case? An example is shown in figure 6 for the two-compartment model, and a much wider range of behavior is found in this case. Simply changing the value of v_{max}^d can produce a single power law tail, a dual regime with an exponential tail, or a dual power law curve with either a steep or a shallow terminal tail. A similar transition between different regimes also occurs when the dose increases, the volume of distribution decreases, or k_{21} increases. Therefore, this situation is much more sensitive to changes in the dosing regimen or patient characteristics. While the asymptotic time-dependence in figures 4, 5 and 6 show a predominantly concave shape hence indicating characteristic Michaelis-Menten saturable kinetics as proposed in our model, these very long-tails still leave open room for more detailed investigation whether this could indeed be fractal Michaelis-Menten kinetics in both compartments, one of them or none. The issue remains open while more accurate empirical data are accumulating in the literature.

Simulations can also be used to investigate the dose-dependence of AUC and C_{max} beyond the current clinically-relevant range. Both parameters exhibit three distinct regions of dose-dependence on a log-log plot (see figure 7). In both cases, the initial and terminal regions are characterized by approximately $\beta = 1$ (see table 6), indicating linear kinetics when the system is well below or well above the saturable concentration range. The intermediate regions, however, are characterized by a transition to a nonlinear regime with $\beta > 1$. The curves in figure 6 fall within this dose range. Because the onset dose of the intermediate slope is higher for AUC

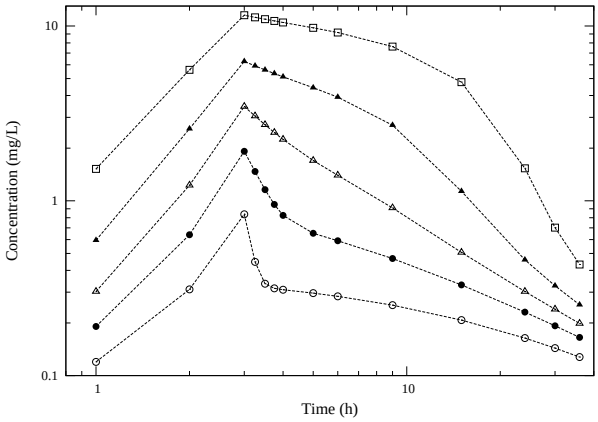

FIGURE 6. The effect of the dose on the shape of the concentration versus time curve for a hypothetical two-compartment model with $K_M^d << K_M^e$. Open circles, 40 mg; solid circles, 50 mg; open triangles, 60 mg; solid triangles, 75 mg; open squares, 100 mg. The model parameters are given in column 2 of table 5.

TABLE 6. The power law exponent β describing the graphs in figure 7.

AUC		
Dose Range (mg)	β	R^2
$0-10$	1.050(0.006)	1.000
$55-300$	3.163(0.005)	1.000
>400	1.0683(0.0004)	1.000
C_{max}		
Dose Range (mg)	β	R^2
$0-10$	1.066(0.009)	1.000
$20-60$	3.67(0.01)	1.000
>150	1.0202(0.0001)	1.000

than for C_{max}, and the slope persists over a longer range, there appears to be a lag between the occurrence of disproportionately higher maximum concentrations and an overall noticeable effect on the shape of the concentration versus time curve. In summary, power law analysis is helpful in predicting nonlinear kinetics, and figure 7 emphasizes that the concept of linearity is valid only over a specified dose range.

Additional simulations were performed to investigate whether a relationship exists between β and α, such that the nonlinear dose-dependence of AUC and C_{max} is correlated with the non-exponential shape of the long-time tail. Figure 8 shows that β increases as α decreases; therefore the dose-dependence becomes increasingly disproportionate as the long-time tail becomes more shallow. In other words, the greater the contribution that the tail portion of the curve makes to the overall AUC, the greater the increase in AUC with an increase in dose.

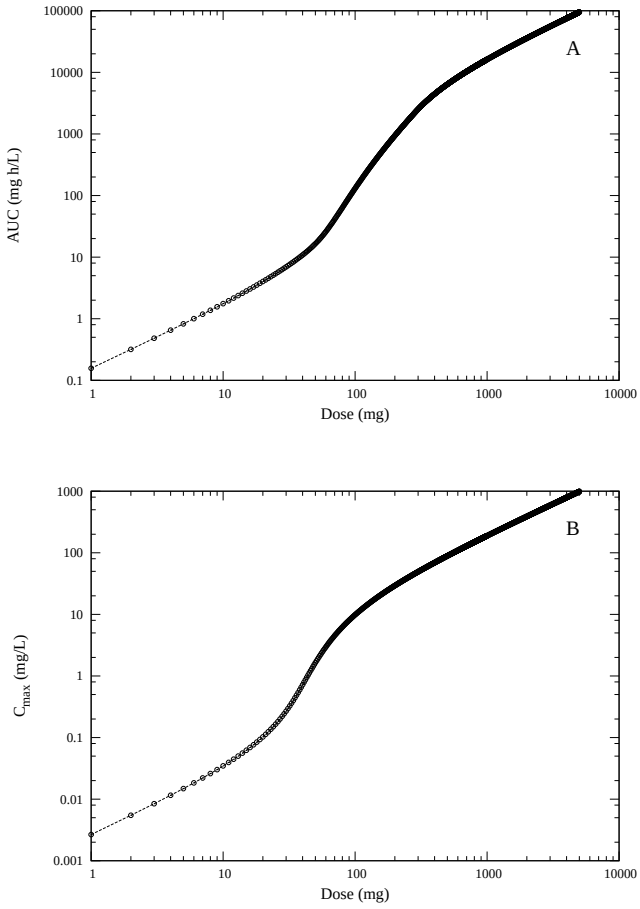

FIGURE 7. The dose-dependence of (A) AUC and (B) C_{max}. The model parameters are given in column 2 of table 5.

Having confirmed the qualitative correctness, through numerical simulations, of the saturable two-compartment model and the underlying pharmacokinetic equations, we now intend to examine the possibility of obtaining some analytical solutions to the problem, which would allow for not only data fitting exercises but also predictive statements to be generated.

3.3. **Analytical solutions.** One of the advantages of obtaining semi-analytical solutions is that different infusion rates and dosage rates can be analyzed and these quantities can be optimized before giving the drug to patients. As stated earlier, the third compartment does not have a significant impact on the mathematical modeling of paclitaxel. Thus, to make the problem more tractable, we shall concentrate on analytical solutions of the saturable two-compartment model. Setting $k_{13} = k_{31} = 0$, we obtain two coupled differential equations, equations 9 and 10, which can be shown to be equivalent to a single second order nonlinear differential equation;

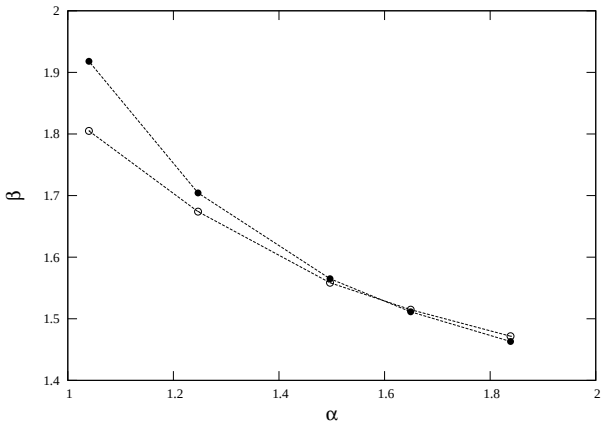

FIGURE 8. The relationship between β and α for a three-compartment model. The value for β was determined for three-hour infusions of 135, 175, 200, 250, and 300 mg/m^2 of paclitaxel. Open circles, AUC; solid circles, C_{max}. The model parameters are given in column 1 of table 5 except for the parameter v^d_{max}, which varied between $5.1 mgL^{-1}h^{-1}$ and $20.4 mgL^{-1}h^{-1}$.

$$0 = \ddot{C}_1 + \left[\frac{v^d_{max}K^d_M}{(K^d_M + C_1)^2} + k_{21} + \frac{v^e_{max}K^e_M}{(K^e_M + C_1)^2}\right]\dot{C}_1 + \frac{v^e_{max}k_{21}C_1}{K^e_M + C_1} - \frac{1}{V_d}\left[k_{21}i(t) + \frac{di(t)}{dt}\right]. \tag{12}$$

The drug concentration in compartment two is obtained using the relationship given by equation 9 once the drug concentration in the blood plasma is known by solving equation 12.

3.3.1. *LOW CONCENTRATION SOLUTION.* When the drug concentration becomes sufficiently small, then equations 9 and 10 are linear and are of the form;

$$\dot{C}_1 = -\frac{v^d_{max}C_1}{K^d_M} + k_{21}C_2 - \frac{v^e_{max}C_1}{K^e_M} + \frac{i(t)}{V_d}, \tag{13}$$

$$\dot{C}_2 = \frac{v^d_{max}C_1}{K^d_M} - k_{21}C_2. \tag{14}$$

The linear version of equation 12 is;

$$\ddot{C}_1 + \left[\frac{v^d_{max}}{K^d_M} + k_{21} + \frac{v^e_{max}}{K^e_M}\right]\dot{C}_1 + \frac{v^e_{max}k_{21}C_1}{K^e_M} = \frac{1}{V_d}\left[k_{21}i(t) + \frac{di(t)}{dt}\right]. \tag{15}$$

The advantage of studying the linear regime is because of the applicability to cases where the patient requires a low dosage or to understand the long-term concentrations of the drug in the body, which gives an indication of when the next round of chemotherapy can begin.

The solution to the linear equation for the drug concentration in the blood plasma is the sum of two exponential solutions plus a solution due to the infusion of the

drug into the system given by;

$$C_1(t) = A_- e^{-t\Delta_-} + A_+ e^{-t\Delta_+} + \int_{t_o}^{t} d\tau \frac{i(\tau)}{V_d(\Delta_+ - \Delta_-)} \times \left[[\Delta_+ - k_{21}]\, e^{\Delta_+(\tau - t)} - [\Delta_- - k_{21}]\, e^{\Delta_-(\tau - t)} \right], \tag{16}$$

where A_- and A_+ are determined from the initial conditions at time t_0, and

$$\Delta_\pm = \frac{1}{2}\left[\frac{v^d_{max}}{K^d_M} + \frac{v^e_{max}}{K^e_M} + k_{21} \right] \pm \sqrt{\frac{1}{4}\left[\frac{v^d_{max}}{K^d_M} + \frac{v^e_{max}}{K^e_M} + k_{21} \right]^2 - \frac{k_{21} v^e_{max}}{K^e_{max}}} \tag{17}$$

Consider the special case when there is initially no drug in the system and there is a constant intravenous infusion, i_o, from time $t = t_0$ to time $t = t_1$. The solution given by equation 16 becomes;

$$C_1 = \begin{cases} 0, & t < t_0 \\ i_0 \left[\frac{[\Delta_+ - k_{21}](1 - e^{-(t-t_0)\Delta_+})}{\Delta_+ V_d(\Delta_+ - \Delta_-)} - \frac{[\Delta_- - k_{21}](1 - e^{-(t-t_0)\Delta_-})}{\Delta_- V_d(\Delta_+ - \Delta_-)} \right], & t_0 < t < t_1. \\ A^{(1)}_- e^{-t\Delta_-} + A^{(1)}_+ e^{-t\Delta_+}, & t > t_1 \end{cases} \tag{18}$$

The two parameters, $A^{(1)}_-$ and $A^{(1)}_+$ are determined from the boundary conditions that $C_1(t)$ and $C_2(t)$ are continuous at time $t = t_1$. The solution in equation 18 has been written in a form that already satisfies the initial conditions and the boundary conditions at time $t = t_0$.

The solution given by equation 18 was fitted to the experimental data in figure 2. In particular, we set $t_0 = 0h$ and $t_1 = 3h$ and used the 225 mg/m^2 data for time $t > 3h$. The fit to the experimental data gives $\Delta_- = 0.219$ and $\Delta_+ = 1.772$; or in terms of the original model parameters:

$$\begin{aligned} \frac{v^d_{max}}{K^d_M} &= 0.410h^{-1} \\ \frac{v^e_{max}}{K^e_M} &= 1.277h^{-1}. \\ k_{21} &= 0.304h^{-1} \end{aligned} \tag{19}$$

Figure 9 shows the linear solution given in equation 18 using the two sets of parameters given in table 5 as well as the best-fit parameters given in equation 19. Figure 9a shows the experimental data and the solution given by equation 18 with the parameters given by equation 19. Figures 9b and 9c illustrate how poorly the linear solution given by equation 18 with the parameters given in columns 1 and 2 of table 5 fits the experimental data. It is quite clear that the linear model is inadequate to represent the experimental data except for figure 9a in which a set of parameters were chosen for the best fit. However, even then the fit is not good. Moreover, even in figure 9a, the long-time (more than 10 hours) tail drops off much more rapidly than in the experimental concentration versus time curve.

3.3.2. *HIGH CONCENTRATION SOLUTION.* When the concentration becomes sufficiently large, equations 9 and 10 are approximately linear and are of the form;

$$\dot{C}_1 = -v^d_{max} + k_{21} C_2 - v^e_{max} + \frac{i(t)}{V_d} \tag{20}$$

$$\dot{C}_2 = v^d_{max} - k_{21} C_2. \tag{21}$$

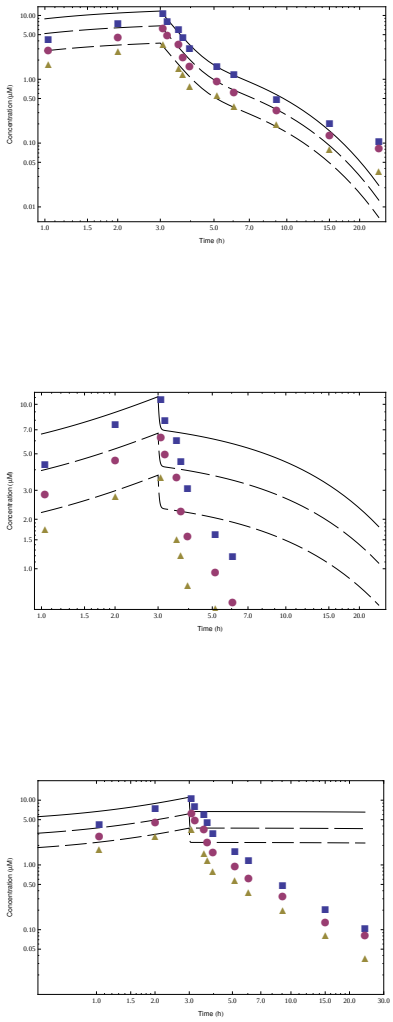

FIGURE 9. Concentration (μM) versus time (h) pharmacokinetic data for three-hour infusions of paclitaxel, replotted from Kearns *et al.* [26] for three dose levels. (triangles, 135 mg/m^2; circles, 175 mg/m^2; squares, 225 mg/m^2). (A) Log-log plot showing a fit to the linear solution with the parameters given in equation 19. (B) Log-log plot of the linear solution with the parameters given in column 1 of table 5. (C) Log-log plot of the linear solution with the parameters given in column 2 of table 5.

The solution of these equations for the blood plasma concentration is;

$$C_1(t) = C_1(t_0) + \left[C_2(t_0) - \frac{v^d_{max}}{k_{21}}\right](1 - e^{-k_{21}(t-t_0)}) - v^e_{max}(t - t_0) + \int_{t_0}^{t} d\tau \frac{i(\tau)}{V_d}. \quad (22)$$

Interestingly, this solution has both a term with linear time dependence and a term with exponential time dependence. In the case when the infusion is zero, the solution given by equation 22 was fitted to the experimental data in figure 2. In particular, we set $t_0 = 0\ h$, $t_1 = 3\ h$ and used the 225 mg/m^2 data for $t > 3\ h$. The fit gives

$$\begin{aligned} v^e_{max} &= 0.052\ \mu M\ h^{-1} \\ k_{21} &= 1.239\ h^{-1} \end{aligned} \quad (23)$$

Figure 10 compares the experimental data with the solution given in equation 22. Figure 10a shows the solution given by equation 22 using the parameters given in equation 23. Figures 10b and 10c show the solution given by equation 22 using the parameters given in column 1 and column 2 of table 5, respectively. The solution gives an excellent fit for large concentrations of drug in the blood plasma, where we would expect the solution to be valid. In fact, if we focus only on the high concentration experimental data from the third hour to the fourth hour, where the solution given by equation 22 should be valid then figure 10c has the best fit to the data.

3.3.3. *EXACT SOLUTION.* The low concentration linear solution has exponential time dependence whereas the high concentration solution has both a term with exponential time dependence and a term with a power law time dependence. We, therefore, expect the exact solution to be a combination of both powers of time and exponentials of time. This section looks at obtaining an exact analytical solution to the two-compartment nonlinear saturable model. Equation 9 gives the solution for $C_2(t)$, if we know the concentration in the blood, $C_1(t)$, which satisfies equation 12. Therefore, we need to solve equation 12 and we are interested in two situations; (i) when there is a constant infusion rate such as an intravenous infusion, and (ii) when the concentration of drug in the system decays in the body through the elimination organs. The infusion is assumed to be zero before time t_0, a nonzero constant from time t_0 until t_1, and zero after time t_1. In addition, the initial conditions are assumed to be $C_1(t_0) = C_2(t_0) = 0$. The solution for the drug concentration in the blood plasma can be written in terms of parametric functions, as follows;

$$C_1(t) = \begin{cases} 0 & , t < t_0 \\ C_1^{max} x & , t_0 < t < t_1,\ 0 < x < 1. \\ C_1^{max}(1 - y) & , t_1 < t,\ 0 < y < 1 \end{cases} \quad (24)$$

The parametric functions x and y are restricted to have a value bounded between zero and one. The parametric function x is zero when the infusion begins and is one when the infusion stops. The parameter function y is zero when the infusion stops and approaches one as the time goes to infinity. With these constraints on the parametric functions x and y, it is clear that equation 24 satisfies the boundary conditions for the drug concentration in the blood plasma.

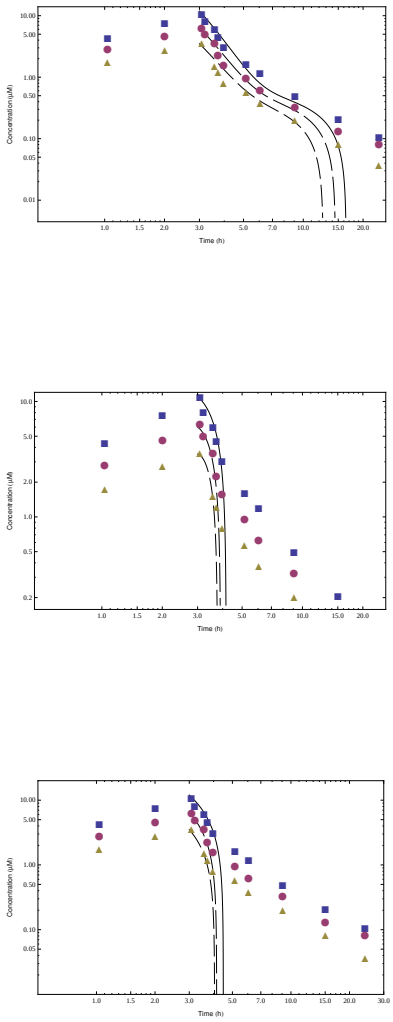

FIGURE 10. Concentration (μM) versus time (h) pharmacokinetic data for three-hour infusions of paclitaxel, replotted from Kearns *et al.* [26] for three dose levels. (triangles, 135 mg/m^2; circles, 175 mg/m^2; squares, 225 mg/m^2). (A) Log-log plot showing a fit to the solution in equation 22 with the parameters given in equation 23. (B) Log-log plot of the solution in equation 22 with the parameters given in column 1 of table 5. (C) Log-log plot of the solution in equation 22 with the parameters given in column 2 of table 5.

In order to determine the parametric functions, the rate of change of the drug concentration in the blood plasma is assumed to have the functional form;

$$\dot{C}_1(t) = \begin{cases} C_1^{max}\dot{x} & = \frac{C_1^{max}a_0}{1+\sum_{n=1}^{\infty} b_n x^n} & , t_0 < t < t_1 \\ -C_1^{max}\dot{y} & = \frac{-C_1^{max}\sum_{n=0}^{\infty} c_n(1-y)^{n+1}}{\sum_{n=0}^{\infty}(n+1)a_1 c_n(1-y)^n} & , t_1 < t \end{cases} . \tag{25}$$

The time variable can be expressed in terms of the parametric functions by integrating equation 25;

$$t = \begin{cases} t_0 + \frac{1}{a_0}\left[x + \sum_{n=1}^{\infty}\frac{b_n x^{n+1}}{n+1}\right] & , t_0 < t < t_1 \\ t_1 - a_1 \ln\left[\frac{\sum_{n=1}^{\infty} c_n(1-y)^{n+1}}{\sum_{n=0}^{\infty} c_n}\right] & , t_1 < t \end{cases} . \tag{26}$$

The solution for the concentration in compartment 2, which is given by equation 9, becomes;

$$C_2 = \frac{1}{k_{21}} \begin{cases} \frac{v_{max}^d C_1^{max} x}{K_M^d + C_1^{max} x} + \frac{v_{max}^e C_1^{max} x}{K_M^e + C_1^{max} x} + \frac{C_1^{max} a_0}{1+\sum_{n=1}^{\infty} b_n x^n} - \frac{i_0}{V_d}, t_0 < t < t_1 \\ \frac{v_{max}^d C_1^{max}(1-y)}{K_M^d + C_1^{max}(1-y)} + \frac{v_{max}^e C_1^{max}(1-y)}{K_M^e + C_1^{max}(1-y)} - \frac{C_1^{max}\sum_{n=0}^{\infty} c_n(1-y)^{n+1}}{\sum_{n=0}^{\infty}(n+1)a_1 c_n(1-y)^n} \end{cases} . \tag{27}$$

The drug concentration in compartment 2 must also satisfy the boundary conditions when x = 0, x = 1, y = 0 and y = 1. The y = 1 boundary condition is automatically satisfied. The other three boundary conditions are;

$$\begin{aligned} C_1^{max} a_0 &= \frac{i_0}{V_d} && , \ when\ x = 0 \\ k_{21} C_2^{max} &= \frac{v_{max}^d C_1^{max}}{K_M^d + C_1^{max}} + \frac{v_{max}^e C_1^{max}}{K_M^e + C_1^{max}} + \frac{C_1^{max} a_0}{1+\sum_{n=1}^{\infty} b_n} - \frac{i_0}{V_d} && , \ when\ x = 1 \\ k_{21} C_2^{max} &= \frac{v_{max}^d C_1^{max}}{K_M^d + C_1^{max}} + \frac{v_{max}^e C_1^{max}}{K_M^e + C_1^{max}} - \frac{C_1^{max}\sum_{n=0}^{\infty} c_n^{n+1}}{\sum_{n=0}^{\infty}(n+1)a_1 c_n} && , \ when\ y = 0 \end{aligned} \tag{28}$$

Setting $x = 1$ and $t = t_1$ in equation 26, and combined with equation 28 determines the value for the three of the parameters; C_1^{max}, a_0 and a_1:

$$\begin{aligned} C_1^{max} &= \frac{i_0}{a_0 V_d} \\ a_0(t_1 - t_0) &= \left[1 + \sum_{n=1}^{\infty}\frac{b_n}{n+1}\right] \\ \frac{\sum_{n=0}^{\infty} c_n}{\sum_{n=0}^{\infty}(n+1)a_1 c_n} &= \frac{\sum_{n=1}^{\infty} a_0 b_n}{1+\sum_{n=1}^{\infty} b_n} \end{aligned} . \tag{29}$$

The unknown parameters in equation 25 are determined by substitution of equations 24, 25 and 27 into equation 12. The solution of the parametric functions, x and y, gives a unique set of values for the parameters b_n and c_n. The parameter a_1 is the only parameter with multiple values as shown below in equation 30.

$$\begin{aligned} a_1 = 0; \ & \frac{k_{21}K_M^d K_M^e + v_{max}^d K_M^e + v_{max}^e K_M^d}{2v_{max}^e k_{21} K_M^d} \\ & \pm \frac{\sqrt{\left[k_{21}K_M^d K_M^e + v_{max}^d K_M^e + v_{max}^e K_M^d\right]^2 - 4v_{max}^e k_{21}\left(K_M^d\right)^2 K_M^e}}{2v_{max}^e k_{21} K_M^d}. \end{aligned} \tag{30}$$

Equation 26 shows that $1/a_1$ is the decay constant. Therefore, the solution $a_1 = 0$ would produce a concentration that would go instantly to zero as soon as the infusion stops. The other two solutions for a_1 are similar to the decay constants given in equation 17 for the linear solution. Figure 4 shows that the elimination of the drug always starts with a steep slope and then for short infusions goes to a shallower slope. This would appear to be contradictory to the one-hour infusion experimental data; however, the steep slope occurs over a very short period that

possibly was not observed experimentally. The solution in equation 30 with the negative square root gives a steep slope and the solution in equation 30 with the positive square root would give a shallow slope. The expressions for the b_n's and c_n's are given in the appendix where additional details of our derivation are also provided.

In order to understand the solution better, we can look at two limiting cases when the time is greater than t_1. In the first case, the time is very close to when the infusion is turned off and the parametric function y is approximately zero. The second case is when the drug has been allowed to decay for a very long time and the parametric function y is approximately one. Equation 26 in these two cases simplifies to

$$\frac{t-t_1}{-a_1} = \ln\left[\frac{\sum_{n=0}^{\infty} c_n(1-y)^{n+1}}{\sum_{n=0}^{\infty} c_n}\right] \approx \begin{cases} \ln\left[1 - y\frac{\sum_{n=0}^{\infty} c_n(n+1)}{\sum_{n=0}^{\infty} c_n}\right] & ,t \approx t_1 \\ \ln\left[\frac{c_0(1-y)}{\sum_{n=0}^{\infty} c_n}\right] & ,t \to \infty \end{cases}. \quad (31)$$

These two cases reduce equation 24 to

$$\frac{C_1}{C_1^{max}} = 1 - y \approx \begin{cases} 1 - \frac{\sum_{n=0}^{\infty} c_n\left[n+[1+t_1-t]^{1/a_1}\right]}{\sum_{n=0}^{\infty} c_n(n+1)} & ,t \approx t_1 \\ \exp\left[\frac{t-t_1}{-a_1}\right]\sum_{n=0}^{\infty}\frac{c_n}{c_0} & ,t \to \infty \end{cases}. \quad (32)$$

The short-time limit in equation 32 shows a power law time dependence with an exponent of $1/a_1$, which is consistent with the high concentration solution given in equation 22. This power-law behavior is also consistent with the experimental data. The long-time asymptotic limit has an exponential time dependence, which is consistent with both the experimental data and the linear solution given in equation 18. These results are in agreement with the experimental data and the numerical results shown in the previous section.

4. **Conclusion.** In this paper we have developed and analyzed a multi-compartment model applied to the case of pharmacokinetics of paclitaxel. We have demonstrated the appropriateness of this relatively simple model to the numerous data sets found in the literature and found numerical fits to the model parameters. Moreover, we have been able to obtain a number of analytical solutions of the equations underlying the model. Special solutions have been found in several limiting cases including high- and low-concentration values of the drug as well as short- and long-time limits in the general case. Two dominant exponents were found to characterize the pharmacokinetic behavior of paclitaxel following short, intermediate, and long infusion times, suggesting a potential universality class. In addition, the self-similar nature of power laws may imply that pharmacological processes are linked over different time and/or size scales. To date, allometric scaling has been applied to pharmacokinetics to assess interspecies and intraspecies variation in pharmacokinetic parameters, however the scaling of pharmacological processes within an individual has yet to be discussed and warrants further investigation. The results obtained here can be used in the future for predictive purposes as well as for applications of the model to other members of the taxane family. Consequently, the proposed model has general value beyond the case studied in this paper.

In particular, analysis of power law tails of the concentration dependence on time can provide insight into the underlying drug processes as well as valuable information for clinical applications. Based on our rigorous mathematical analysis of the problem discussed in this paper, longer infusions leading to a steeper tail would

theoretically be best for paclitaxel, because that would indicate a greater portion of the drug being transferred to the target tumor tissue. Our recommendation of extending infusion times while simultaneously lowering the maximum concentration is consistent with earlier empirical analyses (see e.g. Verweij *et al.* [60]). Our analysis specifically explains using a detailed mathematical model why this is so and how it can be further optimized in future applications. Hence the recommendations provided here not only have retrospective value but also offer prospective potential. Furthermore, identification of empirical power law tails has important consequences for the calculation of pharmacokinetic measures that are extrapolated back from the tail dependence, and it implies that the concept of a terminal half-life does not apply. An advantage of our proposed generating mechanism for empirical power law tails is that it places no restriction on the value of the exponent α, in contrast to models suggested for the bone-seeking elements, where $-1 < \alpha < 0$ [36] and for fractal kinetics in which $-1 \leq \alpha \leq 0$ and $d_s \leq 2$ [12].

We have shown that two competing saturable processes can generate concentration versus time curves with empirical power law tails. To the best of our knowledge, this is one of the first few studies to report power law tails in the concentration versus time curves of an anticancer drug, and to relate the existence of power law tails to saturable processes. Although a single saturable process cannot produce a power law, two competing saturable processes can produce a range of behavior that includes single and dual power law regimes. Furthermore, although power law tails have been reported for clearance curves, this is the first study to investigate the tails of infusion curves and the dependence of the shape of the curve on the infusion rate.

Before embarking on a full pharmacokinetic analysis, the tails of concentration versus time curves can be checked for a power law fit. The existence of an empirical power law tail, especially a shallow one, can signal dose-dependent behavior. In the case of paclitaxel, a steeper decline is more desirable, since it implies a greater distribution to the tumor tissues as well as a decrease in the extent of nonlinearity.

Acknowledgments. KJEV would like to thank the staff at the Cross Cancer Institute for their hospitality during his visits to Edmonton, Alberta.

REFERENCES

[1] R. Advani, G. A. Fisher, B. L. Lum, J. Hausdorff, J. Halsey, M. Litchman and B. I. Sikic, *A phase I trial of doxorubicin, paclitaxel, and valspodar (PSC 833), a modulator of multidrug resistance*, Clin. Cancer Res., **7** (2001), 1221–1229.

[2] J. Anderson, S. B. Osborn, R. W. Tomlinson and M. A. Weinbren, *Some applications of power law analysis to radioisotope studies in man*, Phys. Med. Biol., **8** (1963), 287–295.

[3] J. B. Bassingthwaighte and D. A. Beard, *Fractal 15O-labeled water washout from the heart*, Circ. Res., **77** (1995), 1212–1221.

[4] D. A. Beard and J. B. Bassingthwaighte, *Power-law kinetics of tracer washout from physiological systems*, Ann. Biomed. Eng., **26** (1998), 775–779.

[5] H. G. Boxenbaum, *Pharmacokinetics tricks and traps: Flip-flop models*, J. Pharm. Pharm. Sci., **1** (1998), 90–91.

[6] T. Brown, K. Havlin, G. Weiss, J. Cagnola, J. Koeller, J. Kuhn, J. Rizzo, J. Craig, J. Phillips and D. Von Hoff, *A phase I trial of taxol given by a 6-hour intravenous infusion*, J. Clin. Oncol., **9** (1991), 1261–1267.

[7] P. Chelminiak, R. E. Marsh, J. A. Tuszyński, J. M. Dixon and K. J. E. Vos, *Asymptotic time dependence in the fractal pharmacokinetics of a two-compartment model*, Phys. Rev. E, **72** (2005), Art. Id 031903, 1–7.

[8] B. Damascelli, G. Cantu, F. Mattavelli, P. Tamplenizza, P. Bidoli, E. Leo, F. Dosio, A. M. Cerrotta, G. Di Tolla, L. F. Frigerio, F. Garbagnati, R. Lanocita, A. Marchiano, G. Patelli, C. Spreafico, V. Ticha, V. Vespro and F. Zunino, *Intraarterial chemotherapy with polyoxyethylated castor oil free paclitaxel, incorporated in albumin nanoparticles (ABI-007): Phase II study of patients with squamous cell carcinoma of the head and neck and anal canal: preliminary evidence of clinical activity*, Cancer, **92** (2001), 2592–2602.

[9] A. Dokoumetzidis and P. Macheras, *Fractional pharmacokinetics and pharmacodynamics*, J. of Pharmacokinetics and Pharmacodynamics, **36** (2009), 165–178.

[10] A. Dokoumetzidis, R. Magin and P. Macheras, *A commentary on fractionalization of multi-compartmental models*, J. of Pharmacokinetics and Pharmacodynamics, **37** (2010), 203–207.

[11] F. Doz, J. C. Gentet, F. Pein, D. Frappaz, P. Chastagner, S. Moretti, G. Vassal, J. Arditti, O. Van Tellingen, A. Iliadis and J. Catalin, *Phase I trial and pharmacological study of a 3-hour paclitaxel infusion in children with refractory solid tumors: A SFOP study*, British Journal of Cancer, **84** (2001), 604–610.

[12] J. Fuite, R. Marsh and J. Tuszyński, *Fractal pharmacokinetics of the drug mibefradil in the liver*, Phys. Rev. E, **66** (2002), Art. Id. 021904, 1–11.

[13] H. Gelderblom, J. Verweij, D. M. van Zomeren, D. Buijs, L. Ouwens, K. Nooter, G. Stoter and A. Sparreboom, *Influence of Cremophor EL on the bioavailability of intraperitoneal Paclitaxel*, Clin. Cancer Res., **8** (2002), 1237–1241.

[14] H. Gelderblom, S. D. Baker, A. Zhao, J. Verwij and A. Sparrreboom, *Distribution of paclitaxel in plasma and cerebrospinal fluid*, Anti-cancer drugs, **14** (2003), 365–368.

[15] K. Gelmon, E. Eisenhauer, C. Bryce, A. Tolcher, L. Mayer, E. Tomlinson, B. Zee, M. Blackstein, E. Tomiak, J. Yau, G. Batist, B. Fisher and J. Iglesias, *Randomized phase II study of high-dose paclitaxel with or without amifostine in patients with metastatic breast cancer*, J. Clin. Oncol., **17** (1999), 3038–3047.

[16] L. Gianni, C. M. Kearns, A. Giani, G. Capri, L. Vigano, A. Lacatelli, G. Bonadonna and M. J. Egorin, *Nonlinear pharmacokinetics and metabolism of paclitaxel and its pharmacokinetic/pharmacodynamic relationships in humans*, J. Clin. Oncol., **13** (1995), 180–190.

[17] M. Gibaldi and D. Perrier, "Pharmacokinetics," 2^{nd} edition, M. Dekker, New York, 1982.

[18] K. Gough, M. Hutchinson, O. Keene, B. Byrom, S. Ellis, L. Lacey and J. McKellar, *Assessment of dose proportionality: report from the statisticians in the pharmaceutical industry/pharmacokinetics UK joint working party*, Drug Inf. J., **29** (1995), 1039–1048.

[19] A. Henningsson, M. O. Karlsson, L. Vigano, L. Gianni, J. Verweij and A. Sparreboom, *Mechanism-based pharmacokinetic model for paclitaxel*, J. Clin. Oncol., **19** (2001), 4065–4073.

[20] M. T. Huizing, V. H. Misser, R. C. Pieters, W. W. ten Bokkel Huinink, C. H. Veenhof, J. B. Vermorken, H. M. Pinedo and J. H. Beijnen, *Taxanes: A new class of antitumor agents*, Cancer Invest., **13** (1995), 381–404.

[21] J. A. Jacquez, "Compartmental Analysis in Biology and Medicine," BioMedware, Ann Arbor, 1996.

[22] M. A. Jordan, R. J. Toso, D. Thrower and D. L. Wilson, *Mechanism of mitotic block and inhibition of cell proliferation by taxol at low concentrations*, Proc. Natl. Acad. Sci. USA, **102** (1993), 9552–9556.

[23] M. A. Jordon and L. Wilson, *Taxane Anticancer Agents: Basic Science and Current Status*, in "ACS Symp. Series 583" (eds. G. Georg, T. Chen, I. Ojima and D. Vyas), The American Chemical Society, Washington, (1995), 138–153.

[24] M. A. Jordan, *Mechanism of action of antitumor drugs that interact with microtubules and tubulin*, Curr. Med. Chem. Anti-Canc. Agents, **2** (2002), 1–17.

[25] M. O. Karlsson, V. Molnar, A. Freijs, P. Nygren, J. Bergh and R. Larsson, *Pharmacokinetic models for the saturable distribution of paclitaxel*, Drug Metab. Dispos., **27** (1999), 1220–1223.

[26] C. M. Kearns, L. Gianni and M. J. Egorin, *Paclitaxel pharmacokinetics and pharmacodynamics*, Semin. Oncol., **22** (1995), 16–23.

[27] T. Y. Kim, D. W. Kim, J. Y. Chung, S. G. Shin, S. C. Kim, D. S. Heo, N. K. Kim and Y. J. Bang, *Phase I and pharmacokinetic study of Genexol-PM, a cremophor-free, polymeric micelle-formulated paclitaxel, in patients with advanced malignancies*, Clin. Cancer Res., **10** (2004), 3708–3716.

[28] K. Kosmidis, V. Karalis, P. Argyrakis and P. Macheras, *Michaelis-Menten kinetics under spatially constrained conditions: Application to mibefradil pharmacokinetics*, Biophys. J., **87** (2004), 1498–1506.

[29] M. Lopez-Quintela and J. Casado, *Revision of the methodology in enzyme kinetics: A fractal approach*, J. Theor. Biol., **139** (1989), 129–139.
[30] T. M. Ludden, S. L. Beal and L. B. Sheiner, *Comparison of the akaike information criterion, the Schwartz criterion and the F-test as guides to model selection*, J. Pharmacokinet. Biopharm., **22** (1994), 431–445.
[31] P. Macheras, *A fractal approach to heterogeneous drug distribution: Calcium pharmacokinetics*, Pharm. Res., **13** (1996), 663–670.
[32] H. Maier-Lenz, B. Hauns, B. Haering, J. Koetting, K. Mross, C. Unger, T. Bauknecht, A. du Bois, H. G. Meerpohl, N. Hollaender and K. Diergarten, *Phase I study of paclitaxel administered as a 1-hour infusion: Toxicity and pharmacokinetics*, Semin. Oncol., **24** (1997), Art. Id. S19, 16–19.
[33] R. E. Marsh and J. A. Tuszyński, *Fractal Michaelis-Menten kinetics under steady state conditions: Application to mibefradil*, Pharm. Res., **12** (2006), 2760–2767.
[34] R. E. Marsh, J. A. Tuszyński, M. B. Sawyer and K. J. E. Vos, *Emergence of power laws in the pharmacokientics of paclitaxel due to competing saturable processes*, J. Pharm. Pharmaceut. Sci., **11** (2008), 77–96.
[35] L. Michaelis and M. L. Menten, *Die kinetik der invertinwirkung*, Biochem. Z., **49** (1913), 333–369.
[36] B. Monsarrat, E. Mariel, S. Cros, M. Gares, D. Guenard, F. Gueritte-Voegelein and M. Wright, *Taxol metabolism. Isolation and identification of three major metabolites of taxol in rat bile*, Drug Metab. Dispos., **18** (1990), 895–901.
[37] T. Mori, Y. Kinoshita, A. Watanabe, T. Yamaguchi, K. Hosokawa and H. Honjo *Retention of paclitaxel in cancer cells for 1 week in vivo and in vitro*, Cancer Chemother. Pharmacol., **58** (2006), 665–672.
[38] K. Mross and N. Hollander and B. Hauns and M. Schumacher and H. Maier-Lenz, *The pharmacokinetics of a 1-h paclitaxel infusion*, Cancer Chemother. Pharmacol., **45** (2000), 463–470.
[39] V. R. Nannan Panday, R. de Wit, J. H. Schornagel, M. Schot, H. Rosing, J. Lieverst, W. W. ten Bokkel Huinink, J. H. Schellens and J. H. Beijnen, *Pharmacokinetics of paclitaxel administered in combination with cisplatin, etoposide and bleomycin in patients with advanced solid tumours*, Cancer Chemother. Pharmacol., **44** (1999), 349–353.
[40] J. H. Nettles, H. Li, B. Cornett, J. M. Krahn, J. P. Snyder and K. H. Downing, *The binding mode of epothilone A on alpha, beta-tubulin by electron crystallography*, Science, **305** (2004), 866–869.
[41] W. P. Norris, S. A. Tyler and A. M. Brues, *Retention of radioactive bone-seekers*, Science, **128** (1958), 456–462.
[42] K. H. Norwich and S. Siu, *Power functions in physiology and pharmacology*, J. Theor. Biol., **95** (1982), 387–398.
[43] T. Ohtsu, Y. Sasaki, T. Tamura, Y. Miyata, H. Nakanomyo, Y. Nishiwaki and N. Saijo, *Clinical pharmacokinetics and pharmacodynamics of paclitaxel: A 3-hour infusion versus a 24-hour infusion*, Clin. Cancer Res., **1** (1995), 599–606.
[44] K. P. Papadopoulos, M. J. Egorin, M. Huang, A. Troxel, E. Kaufman, C. Balmaceda, L. T. Vahdat and C. S. Hesdorffer, *The pharmacokinetics and pharmacodynamics of high-dose paclitaxel monotherapy (825 mg/m2 continuous infusion over 24h) with hematopoietic support in women with metastatic breast cancer*, Cancer Chemother. Pharmacol., **47** (2001), 45–50.
[45] J. Parness and S. B. Horwitz, *Taxol binds to polymerized tubulin in vitro*, J. Cell Biol., **91** (1981), 479–487.
[46] A. Patnaik, E. Warner, M. Michael, M. J. Egorin, M. J. Moore, L. L. Siu, P. M. Fracasso, S. Rivkin, I. Kerr, M. Litchman and A. M. Oza, *Phase I dose-finding and pharmacokinetic study of paclitaxel and carboplatin with oral valspodar in patients with advanced solid tumors*, J. Clin. Oncol., **18** (2000), 3677–3689.
[47] F. Pellegrini and D. R. Budman, *Review: Tubulin function, action of antitubulin drugs, and new drug development*, Cancer Invest., **23** (2005), 264–273.
[48] W. Press, "Numerical Recipes in C: The Art of Scientific Computing," Cambridge University Press, New York, 1992.
[49] D. M. Robinson and G. M. Keating, *Albumin-bound paclitaxel inmetastatic breast cancer drugs*, Drugs, **66** (2006), 941–948.

[50] E. K. Rowinsky, P. J. Burke, J. E. Karp, R. W. Tucker, D. S. Ettinger and R. C. Donehower, *Phase I and pharmacodynamic study of taxol in refractory acute leukemias*, Cancer Res., **49** (1989), 4640–4647.
[51] E. K. Rowinsky, M. Wright, B. Monsarrat, G. J. Lesser and R. C. Donehower, *Taxol: Pharmacology, metabolism and clinical implications*, Cancer Surv., **17** (1993), 283–304.
[52] O. Soepenberg, A. Sparreboom, M. J. de Jonge, A. S. Planting, G. de Heus, W. J. Loos, C. M. Hartman, C. Bowden and J. Verweij, *Real-time pharmacokinetics guiding clinical decisions; phase i study of a weekly schedule of liposome encapsulated paclitaxel in patients with solid tumours*, Eur. J. Cancer, **40** (2004), 681–688.
[53] D. S. Sonnichsen, C. A. Hurwitz, C. B. Pratt, J. J. Shuster and M. V. Relling, *Saturable pharmacokinetics and paclitaxel pharmacodynamics in children with solid tumors*, J. Clin. Oncol., **12** (1994), 532–538.
[54] C. Sottani, C. Minoia, M. D'Incalci, M. Paganini and M. Zucchetti, *High-performance liquid chromatography tandem mass spectrometry procedure with automated solid phase extraction sample preparation for the quantitative determination of paclitaxel (taxol) in humanplasma*, Rapid Commun. Mass Spectrom., **12** (1998), 251–255.
[55] A. Sparreboom, L. van Zuylen, E. Brouwer, W. J. Loos, P. de Bruijn, H. Gelderblom, M. Pillay, K. Nooter, G. Stoter and J. Verweij, *Cremophor EL-mediated alteration of paclitaxel distribution in human blood: Clinical pharmacokinetic implications*, Cancer Res., **59** (1999), 1454–1457.
[56] L. van Zuylen, M. O. Karlsson, J. Verweij, E. Brouwer, P. de Bruijn, K. Nooter, G. Stoter and A. Sparreboom, *Pharmacokinetic modeling of paclitaxel encapsulation in cremophor EL micelles*, Cancer Chemother. Pharmacol., **47** (2001), 309–318.
[57] L. van Zuylen, J. Verweij and A. Sparreboom, *Role of formulation vehicles in taxane pharmacology*, Invest. New Drugs, **19** (2001), 125–141.
[58] D. Verotta, *Fractional compartmental models and multi-term Mittag-Leffler response functions*, Journal of Pharmacokinetics and Pharmacodynamics, **37** (2010), 209–215.
[59] D. Verotta, *Fractional dynamics pharmacokinetics-pharmacodynamic models*, Journal of Pharmacokinetics and Pharmacodynamics, **37** (2010), 257–276.
[60] J. Verweij, M. Clavel and B. Chevalier, *Paclitaxel (taxol) and docetaxel (taxotere): Not simply two of a kind*, Annals of Oncology, **5** (1994), 495–505.
[61] M. Weiss, *Use of gamma distributed residence times in pharmacokinetics*, Eur. J. Clin. Pharmacol., **25** (1983), 695–702.
[62] P. H. Wiernik, E. L. Schwartz, J. J. Strauman, J. P. Dutcher, R. B. Lipton and E. Paietta, *Phase I clinical and pharmacokinetic study of Taxol*, Cancer Res., **47** (1987), 2486–2493.
[63] P. H. Wiernik, E. L. Schwartz, A. Einzig, J. J. Strauman, R. B. Lipton and J. P. Dutcher, *Phase I trial of taxol given as a 24-hour infusion every 21 days: Responses observed in metastatic melanoma*, J. Clin. Oncol., **5** (1987), 1232–1239.
[64] M. E. Wise, S. B. Osborn, J. Anderson and R. W. S. Tomlinson, *A stochastic model for turnover of radiocalcium based on the observed power laws*, Math. Biosci. l, **2** (1968), 199–224.
[65] M. E. Wise, *The evidence against compartments*, Biometrics, **27** (1971), 262.
[66] M. E. Wise, *Interpreting both short and long-term power laws in physiological clearance curves*, Math. Biosci., **20** (1974), 327–337.
[67] M. H. Woo, D. Gregornik, P. D. Shearer, W. H. Meyer and M. V. Relling, *Pharmacokinetics of paclitaxel in an anephric patient*, Cancer Chemother. Pharmacol., **43** (1999), 92–96.

Appendix A. **Exact solution.** This appendix derives an exact analytical solution to the two-compartment nonlinear saturable model. Equation 9 gives the solution for $C_2(t)$, if we know the concentration in the blood, $C_1(t)$, which satisfies equation 12. Therefore, we need to solve equation 12; (i) when there is a constant nonzero infusion rate, and (ii) when the infusion rate is zero. The infusion is assumed to be zero before time t_0, a nonzero constant from time t_0 until t_1, and zero after time t_1. In addition, the initial conditions are assumed to be $C_1(t_0) = C_2(t_0) = 0$. The solution for the drug concentration in the blood plasma can be written in terms of

parametric functions, as follows;

$$C_1(t) = \begin{cases} 0 & ,t < t_0 \\ C_1^{max} x & ,t_0 < t < t_1,\ 0 < x < 1 \\ C_1^{max}(1-y) & ,t_1 < t < \infty,\ 0 < y < 1 \end{cases},$$

which is equation 24.

The parametric function x is zero when the infusion begins and is one when the infusion stops. The parameter function y is zero when the infusion stops and approaches one as the time goes to infinity. Equation 24 satisfies the boundary conditions for the drug concentration in the blood plasma.

In order to determine the parametric functions, the rate of change of the drug concentration in the blood plasma is assumed to have the functional form;

$$\dot{C}_1(t) = \begin{cases} C_1^{max}\dot{x} & = \frac{C_1^{max} a_0}{1+\sum_{n=1}^{\infty} b_n x^n} & ,t_0 < t < t_1 \\ -C_1^{max}\dot{y} & = \frac{-C_1^{max}\sum_{n=0}^{\infty} c_n (1-y)^{n+1}}{\sum_{n=0}^{\infty}(n+1)a_1 c_n (1-y)^n} & ,t_1 < t \end{cases},$$

which is equation 25.

The solution for the concentration in compartment 2, which is given by equation 9, becomes;

$$C_2 = \frac{1}{k_{21}} \begin{cases} \frac{v_{max}^d C_1^{max} x}{K_M^d + C_1^{max} x} + \frac{v_{max}^e C_1^{max} x}{K_M^e + C_1^{max} x} + \frac{C_1^{max} a_0}{1+\sum_{n=1}^{\infty} b_n x^n} - \frac{i_0}{V_d}, t_0 < t < t_1 \\ \frac{v_{max}^d C_1^{max}(1-y)}{K_M^d + C_1^{max}(1-y)} + \frac{v_{max}^e C_1^{max}(1-y)}{K_M^e + C_1^{max}(1-y)} - \frac{C_1^{max}\sum_{n=0}^{\infty} c_n (1-y)^{n+1}}{\sum_{n=0}^{\infty}(n+1)a_1 c_n (1-y)^n}, t_1 < t \end{cases},$$

which is equation 27.

The second derivative of the blood plasma concentration with respect to time is;

$$\frac{\ddot{C}_1(t)}{C_1^{max}} = \begin{cases} \frac{-a_0^2 \sum_{n=1}^{\infty} n b_n x^{n-1}}{\left[1+\sum_{n=1}^{\infty} b_n x^n\right]^3}, t_0 < t < t_1 \\ \frac{\sum_{n=0}^{\infty}\sum_{m=0}^{n}\sum_{k=0}^{n-m}(k+1)(m+1-k)a_1 c_{n-m-k} c_m c_k (1-y)^{n+1}}{\left[\sum_{n=0}^{\infty}(n+1)a_1 c_n (1-y)^n\right]^3} & ,t_1 < t \end{cases}. \quad (33)$$

Substitution of equations 24, 25, 27 and 33 into equation 12,

$$\ddot{C}_1 + \left[\frac{v_{max}^d K_M^d}{(K_M^d + C_1)^2} + k_{21} + \frac{v_{max}^e K_M^e}{(K_M^e + C_1)^2}\right]\dot{C}_1 + \frac{v_{max}^e k_{21} C_1}{K_M^e + C_1} = \frac{1}{V_d}\left[k_{21} i(t) + \frac{di(t)}{dt}\right].$$

gives;

$$\begin{aligned} 0 = {} & \frac{-a_0^2 \sum_{n=1}^{\infty} n b_n x^{n-1}}{\left[1+\sum_{n=1}^{\infty} b_n x^n\right]^3} + \frac{a_0}{1+\sum_{n=1}^{\infty} b_n x^n}\left[\frac{v_{max}^d K_M^d}{(K_M^d + C_1^{max} x)^2} + k_{21}\right. \\ & \left. + \frac{v_{max}^e K_M^e}{(K_M^e + C_1^{max} x)^2}\right] + \frac{v_{max}^e k_{21} x}{K_M^e + C_1^{max} x} - \frac{k_{21} i_0}{V_d C_1^{max}} \end{aligned} \quad (34)$$

and

$$\begin{aligned} 0 = {} & \frac{\sum_{n=0}^{\infty}\sum_{m=0}^{n}\sum_{k=0}^{n-m}(k+1)(m+1-k)a_1 c_{n-m-k} c_m c_k (1-y)^{n+1}}{\left[\sum_{n=0}^{\infty}(n+1)a_1 c_n (1-y)^n\right]^3} \\ & - \frac{\sum_{n=0}^{\infty} c_n (1-y)^{n+1}}{\sum_{n=0}^{\infty}(n+1)a_1 c_n (1-y)^n}\left[\frac{v_{max}^d K_M^d}{(K_M^d + C_1^{max}(1-y))^2} + k_{21}\right. \\ & \left. + \frac{v_{max}^e K_M^e}{(K_M^e + C_1^{max}(1-y))^2}\right] + \frac{v_{max}^e k_{21}(1-y)}{K_M^e + C_1^{max}(1-y)}. \end{aligned} \quad (35)$$

Rearranging equations 34 and 35, we obtain;

$$\begin{aligned} 0 = &- a_0^2 \sum_{n=0}^{\infty} n b_n x^{n-1} + a_0 \left[\sum_{n=0}^{\infty} b_n x^n\right]^2 \left[\frac{v_{max}^d K_M^d}{(K_M^d + C_1^{max} x)^2} + k_{21} \right. \\ &\left. + \frac{v_{max}^e K_M^e}{(K_M^e + C_1^{max} x)^2}\right] + \left[\frac{v_{max}^e k_{21} x}{K_M^e + C_1^{max} x} - \frac{k_{21} i_0}{V_d C_1^{max}}\right] \left[\sum_{n=0}^{\infty} b_n x^n\right]^3, \end{aligned} \tag{36}$$

where $b_0 = 1$, and

$$\begin{aligned} 0 = &\sum_{n=0}^{\infty} \sum_{m=0}^{n} \sum_{k=0}^{n-m} (k+1)(m+1-k) a_1 c_{n-m-k} c_m c_k (1-y)^n - \sum_{n=0}^{\infty} c_n (1-y)^n \\ &\left[\sum_{n=0}^{\infty} (n+1) a_1 c_n (1-y)^n\right]^2 \left[\frac{v_{max}^d K_M^d}{(K_M^d + C_1^{max}(1-y))^2} + k_{21} \right. \\ &\left. + \frac{v_{max}^e K_M^e}{(K_M^e + C_1^{max}(1-y))^2}\right] + \frac{v_{max}^e k_{21} \left[\sum_{n=0}^{\infty} (n+1) a_1 c_n (1-y)^n\right]^3}{K_M^e + C_1^{max}(1-y)}. \end{aligned} \tag{37}$$

In equation 37, the terms with the lowest power of 1-y are;

$$K_M^d K_M^e a_1 - \left[k_{21} K_M^d K_M^e + v_{max}^d K_M^e + v_{max}^e K_M^d\right] a_1^2 + k_{21} v_{max}^e K_M^d a_1^3 = 0. \tag{38}$$

Equation 38 is satisfied by solving for the parameter a_1, namely;

$$\begin{aligned} a_1 = &0; \frac{k_{21} K_M^d K_M^e + v_{max}^d K_M^e + v_{max}^e K_M^d}{2 v_{max}^e k_{21} K_M^d} \\ &\pm \frac{\sqrt{\left[k_{21} K_M^d K_M^e + v_{max}^d K_M^e + v_{max}^e K_M^d\right]^2 - 4 v_{max}^e k_{21} \left(K_M^d\right)^2 K_M^e}}{2 v_{max}^e k_{21} K_M^d}, \end{aligned} \tag{39}$$

which is equation 30.

The solutions to equations 36 and 37 requires reducing the product of sums into a single sum over x and y.

$$\begin{aligned} 0 = &- a_0^2 \sum_{n=0}^{\infty} (n+1) b_{n+1} x^n + a_0 \sum_{n=0}^{\infty} \sum_{m=0}^{n} b_{n-m} b_m x^n \left[\frac{v_{max}^d K_M^d}{(K_M^d + C_1^{max} x)^2} + k_{21} \right. \\ &\left. + \frac{v_{max}^e K_M^e}{(K_M^e + C_1^{max} x)^2}\right] + \sum_{n=0}^{\infty} \sum_{m=0}^{n} \sum_{k=0}^{n-m} b_{n-m-k} b_m b_k k_{21} x^n \left[\frac{v_{max}^e x}{K_M^e + C_1^{max} x} \right. \\ &\left. - \frac{i_0}{V_d C_1^{max}}\right] \end{aligned} \tag{40}$$

and

$$\begin{aligned} 0 = &\sum_{n=0}^{\infty} w^n \sum_{m=0}^{n} \sum_{k=0}^{n-m} (k+1) a_1 c_{n-m-k} c_m c_k \left\{\left[\frac{v_{max}^e k_{21}}{K_M^e + C_1^{max} w}\right] (m+1) a_1^2 \right. \\ &(n+1-m-k) + m + 1 - k - (m+1) a_1 \left[k_{21} + \frac{v_{max}^d K_M^d}{(K_M^d + C_1^{max} w)^2} \right. \\ &\left.\left. + \frac{v_{max}^e K_M^e}{(K_M^e + C_1^{max} w)^2}\right]\right\}, \end{aligned} \tag{41}$$

where w = 1 - y.

Finally, we rearrange each of the terms in equations 40 and 41 so that all the terms with a common power of x or w can be combined.

$$\begin{aligned}0 =& -\sum_{n=0}^{\infty} x^n (n+1) a_0^2 b_{n+1} (K_M^d + C_1^{max} x)^2 (K_M^e + C_1^{max} x)^2 \\ &+ \sum_{n=0}^{\infty} \sum_{m=0}^{n} x^n a_0 b_{n-m} b_m \left[v_{max}^e K_M^e (K_M^d + C_1^{max} x)^2 + k_{21} (K_M^d + C_1^{max} x)^2 \right. \\ &\left. (K_M^e + C_1^{max} x)^2 + v_{max}^d K_M^d (K_M^e + C_1^{max} x)^2 \right] \\ &+ \sum_{n=0}^{\infty} \sum_{m=0}^{n} \sum_{k=0}^{n-m} x^n b_{n-m-k} b_m b_k k_{21} (K_M^e + C_1^{max} x)(K_M^d + C_1^{max} x)^2 \\ &\left[v_{max}^e x - \frac{i_0 (K_M^e + C_1^{max} x)}{V_d C_1^{max}} \right]\end{aligned} \tag{42}$$

and

$$\begin{aligned}0 =& \sum_{n=0}^{\infty} w^n \sum_{m=0}^{n} \sum_{k=0}^{n-m} (k+1) a_1 c_{n-m-k} c_m c_k \left\{ (n+1-m-k)(m+1) a_1^2 v_{max}^e \right. \\ & k_{21} (K_M^d + C_1^{max} w)^2 (K_M^e + C_1^{max} w) + (K_M^d + C_1^{max} w)^2 (K_M^e + C_1^{max} w)^2 \\ & (m+1-k-(m+1) a_1 k_{21}) - (m+1) a_1 \left[v_{max}^d K_M^d (K_M^e + C_1^{max} w)^2 \right. \\ & \left. \left. + v_{max}^e K_M^e (K_M^d + C_1^{max} w)^2 \right] \right\}.\end{aligned} \tag{43}$$

The coefficient of each power of x and w in equations 42 and 43 must vanish, so that $A_n x^n = 0$ and $B_n w^n = 0$ for each n. Also, recall that we have the constraint, $b_0 = 1$.

As an example, consider the case $n = 0$, then $A_0 x^0 = 0$ gives

$$b_1 = \frac{k_{21} K_M^d K_M^e + v_{max}^d K_M^e + v_{max}^e K_M^d}{a_0 K_M^d K_M^e} - \frac{i_0 k_{21}}{a_0^2 V_d C_1^{max}} \tag{44}$$

and $B_0 w^0 = 0$ gives

$$\begin{aligned}a_1 =& 0; \frac{k_{21} K_M^d K_M^e + v_{max}^d K_M^e + v_{max}^e K_M^d}{2 v_{max}^e k_{21} K_M^d} \\ & \pm \frac{\sqrt{\left[k_{21} K_M^d K_M^e + v_{max}^d K_M^e + v_{max}^e K_M^d \right]^2 - 4 v_{max}^e k_{21} \left(K_M^d \right)^2 K_M^e}}{2 v_{max}^e k_{21} K_M^d},\end{aligned} \tag{45}$$

which is equation 30. Similar expressions are obtained for b_{n+1} and a_{n+1} from the nth term.

Received March 5, 2010; Accepted August 22, 2010.

E-mail address: JAT: jackt@ualberta.ca
E-mail address: KJEV: k.vos@uleth.ca
E-mail address: REM: rebeccah.e.marsh@gmail.com
E-mail address: MS: Michael.Sawyer@albertahealthservices.ca